Ferromagnetic materials for MEMS- and NEMS-devices

A. Weddemann*, J. Jadidian, Y.S. Kim, S.R. Khushrushahi, M. Zahn

Research Laboratory of Electronics, Massachusetts Institute of Technology,
77 Massachusetts Ave, MA 02139, USA

*Corresponding author, e-mail: weddeman@mit.edu

ABSTRACT

The calculation of ferromagnetic materials is a challenging task of high industrial and academic impact. The dynamics of a magnetization distribution are governed by the *Landau-Lifshitz-Gilbert* equations which are implemented into COMSOL Multiphysics and solved for assemblies of magnetic nanoparticles and thin film systems. We will discuss various simplifications of the full set of equations for these particular cases and also address the implementation of FEM-BEM methods for a numerically efficient way to evaluate the magnetic stray field without the employment of additional auxiliary domains.

Keywords: ferromagnetism, Landau-Lifshitz-Gilbert equation, hysteresis, hybrid FEM-BEM method

1 INTRODUCTION

Modern hard drives allow for high data storage capacities. Recently, Seagate announced the release of a new model with a storage density of 625 GByte per square inch. In order to push this limit even further and to design novel technologies with even higher data capacities, a strong understanding of the driving dynamics within these systems is required. The data storage process is based on a physical phenomenon known as *giant magnetoresistance* (GMR)-effect [1], [2].

In general, a magnetoresistive effect describes a dependency of the electric resistance on the microscopic magnetic configuration. A simple example where such a behavior can be observed is shown in Figure 1. Two ferromagnetic layers are separated by a non-magnetic conducting spacer. The electric resistance of the device depends on the relative orientation of the magnetization distributions in each layer. A parallel alignment results in a low electric resistance, an antiparallel configuration in a high value. These two resistance states may be interpreted as the bit states `0` and `1`. For applications in data storage devices, a hard switching characteristic, i.e. a high coercive field, is required to guarantee the stability of the magnetic state against thermal effects and, thus, providing a long life time of the stored information.

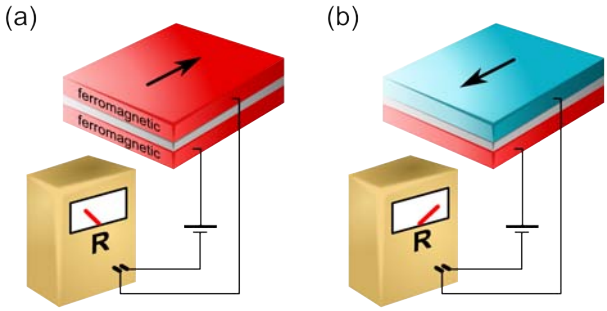

Figure 1: Spintronic device consisting of multiple magnetic layers separated by a non-magnetic spacer. The electric resistance of the device depends on the relative orientation in upper and lower electrode and is (a) low for a parallel alignment and (b) high for an antiparallel configuration.

The origin of this effect can be found in a quantum mechanic interaction between different spin states which results in an increased electron scattering probability (and, therefore, increased electric resistance) for antiparallel spin orientations. Therefore, this type of device is usually called a *spintronic device*. Nowadays, this technology has found many applications beyond data storage. Especially, the area of magnetoresistive sensors is a rapidly growing field. However, if these sensors are capable of detecting even very small fields and field variations, a very soft response is required [3].

In order to reliably predict the characteristic behavior of a magnetoresistive spintronic device and to tailor its properties to specific functional tasks, we need a framework for the numerical calculation of ferromagnetic materials. In this work, we focus on the most relevant cases: thin films and magnetic nanoparticles. From a formal point of view, these systems are of reduced dimensionality and may be approximated by two- and zero-dimensional arrays. However, the demagnetization field does not lose its three-dimensional characteristics. Depending on the type of system, we will explain different strategies to reduce the dimensionality of the magnetic objects without neglecting the full three-dimensional nature of the magnetic field.

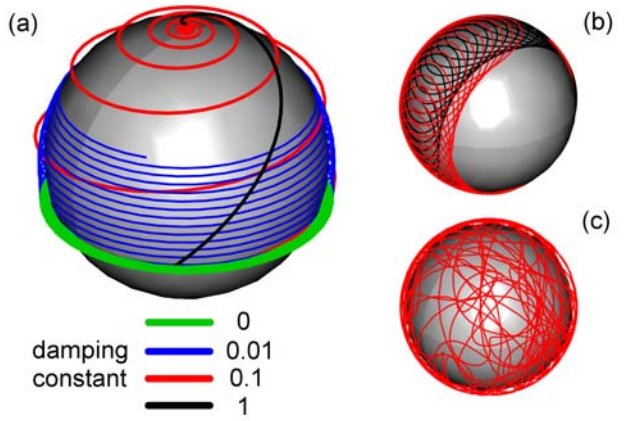

Figure 2: (a) Dynamic behaviour of a magnetic moment $\mathbf{m}$ in an external magnetic field $\mathbf{H}$ parallel to the z-axis for different values of the damping constant α. The green line corresponds to an undamped system, $\alpha = 0$, the path of the magnetic moment forms a closed loop. (b) Trajectories of two interacting magnetic moments and (c) trajectory of one magnetic moment interacting with multiple moments ordered in a cubic lattice grid.

2 GOVERNING EQUATIONS

To find the dynamic equations that govern the magnetic relaxation from an initial to the equilibrium state, let us consider a magnetic moment vector $\mathbf{m}$ brought into an external magnetic field $\mathbf{H}$. The moment vector feels a torque $\mu_0 \mathbf{m} \times \mathbf{H}$ and, consequently, begins to precess around the field axis. The vector orientation changes in respect to time according to

$$\frac{d\mathbf{m}}{dt} = -\gamma \mathbf{m} \times \mathbf{H} \tag{1}$$

with γ the gyromagnetic ratio. With a constant absolute value $|\mathbf{m}|$, we may visualize the trajectory of the moment as a curve on the surface of the three-dimensional sphere with radius $|\mathbf{m}|$. A solution of equation (1) is shown in Figure 2(a), green line. During this precession, the angle between magnetic vector and field axis remains constant indicating a constant total energy $-\mu_0 \mathbf{m} \cdot \mathbf{H}$.

On the microscale, various effects result in an effective damping of the rotation. All contributions of *local* nature, such as phenomena related to electron scattering, can be summarized in an additional phenomenological damping term

$$\frac{d\mathbf{m}}{dt} = -\gamma \mathbf{m} \times \mathbf{H} + \alpha \mathbf{m} \times \frac{d\mathbf{m}}{dt}. \tag{2}$$

The dimensionless damping parameter α may be compared to the viscosity η in a viscous flow imposing a resistance against the motion of the magnetic vector. Since it summarizes a wide range of phenomena, its actual value is commonly unknown. Figure 2(a) shows solutions of equation (2) for different values of α.

In principal, equation (2) is already the governing law. However, we are not interested in a point dipole but in continuous matter. Such matter may be understood as an ensemble of magnetic dipoles where the local dipole density or *magnetization* $\mathbf{M} = M_\mathrm{S}\hat{\mathbf{m}}$ is a vector of a constant length, the *saturation magnetization*, which is a material property. In this continuum model, the microscopic structure such as the coupling between adjacent spin moments, can be taken into account by different contributions to an effective magnetic field $\mathbf{H} \to \mathbf{H}_\mathrm{eff}$. Commonly, the following decomposition is chosen

$$\mathbf{H}_\mathrm{eff} = -\frac{2A}{\mu_0 M_\mathrm{S}} \Delta \hat{\mathbf{m}} + \frac{1}{\mu_0 M_\mathrm{S}} \frac{\delta f_\mathrm{ani}}{\delta \hat{\mathbf{m}}} + \mathbf{H}_\mathrm{d} + \mathbf{H}_\mathrm{ex}. \tag{3}$$

Not all of these terms may be immediately recognized as magnetic fields. However, they all affect a magnetic moment vector in the way that they result in a torque-like contribution $\mu_0 \mathbf{m} \times \mathbf{H}$. The first summand refers to *magnetic exchange energy*, an interatomic coupling due to an overlap of the atomic orbitals (such as the $3d$-orbitals for Iron, Cobalt or Nickel) which leads to a torque density entailing a parallel alignment of contiguous magnetic material. The exchange constant A may, therefore, be regarded as a measure for the magnetic stiffness of a material since the total energy is increased whenever the magnetic distribution reaches a high curvature ΔM_i.

Due to the microscopic crystallographic structure, certain directions of the magnetic vector may be energetically more favorable than other ones which is taken into account by the second term referring to *magnetocrystalline anisotropy energy*. f_ani denotes the anisotropy functional which depends on the polar coordinates of the unit vector $\hat{\mathbf{m}}$. Energy functionals of first order for uniaxial and cubic symmetries are given by

$$f_\mathrm{ani}^\mathrm{uni} = K_\mathrm{u} \left(1 - \left\langle \hat{\mathbf{m}}, \hat{\mathbf{k}} \right\rangle^2\right) \tag{4}$$

$$f_\mathrm{ani}^\mathrm{cub} = K_\mathrm{c} \left(\hat{m}_x^2 \hat{m}_y^2 + \hat{m}_y^2 \hat{m}_z^2 + \hat{m}_z^2 m_x^2\right), \tag{5}$$

with $K_\mathrm{u}, K_\mathrm{c}$ anisotropy constants and $\hat{\mathbf{k}}$ the direction of the easy axis. Examples are shown in Figure 3.

The remaining two contributions refer to the sum over all external magnetic fields $\mathbf{H}_\mathrm{ex}$ and the *demagnetization field* $\mathbf{H}_\mathrm{d}$. The latter one follows the laws of magnetostatics and may, therefore, be expressed as $\mathbf{H}_\mathrm{d} = -\nabla\varphi$, with a magnetic scalar potential φ that may be obtained as a solution of the inhomogeneous Laplace equation

$$\Delta\varphi = \nabla \cdot \mathbf{M} \quad \forall \mathbf{r} \in \mathbb{R}^n \tag{6}$$

$$\frac{\partial\varphi}{\partial\hat{\mathbf{n}}} = \hat{\mathbf{n}} \cdot \mathbf{M} \quad \forall \mathbf{r} \in \Gamma_\mathrm{mag} \tag{7}$$

where Γ_mag denotes the interface between magnetic object and the surrounding space or, in more general terms,

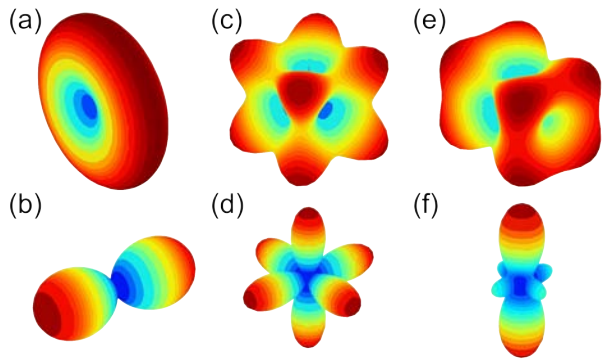

Figure 3: Various energy surfaces for different magnetocrystalline anisotropy scenarios, blue and red areas correspond to energy minima (*easy* axes/planes) and maxima (*hard* axes/planes), respectively. Uniaxial symmetries with either (a) an easy axis or (b) an easy plane, cubic symmetries (c), (d) and combined cases (e), (f).

the interface between two objects of different magnetization. This completes the set of equations for the continuous model. The system (2) to (7) is called *Landau-Lifshitz-equation* [4].

In systems with a high aspect ratio, out-of-plane contributions are usually small when the global configuration is considered, $||m_\perp||_{L^2} \approx 0$, (exceptions can be found in systems with a high perpendicular anisotropy, see e.g. [5]). Under the additional constraint of a constant length of the magnetization vector, the magnetic state is described by the angular in-plane component. Therefore, for this type of analysis, a circular colorcode is employed for the visualization of the vector field where each color indicates the local direction of $\hat{\mathbf{m}}$, Figure 4.

Out of these contributions, the demagnetization field is of non-local nature, i.e., for the evaluation of equation (3) at a certain space point, not only the physical properties at the respective point are required but also the field values in the entire space need to be calculated. As a rule of thumb, an additional auxiliary domain of radius given by five times the geometrical size scale of the investigated structure is sufficient to reach a numerical error that may be neglected. All calculations presented in this work were obtained by the introduction of such an auxiliary domain. More advanced methods such the implementation of a hybrid FEM-BEM approach are currently under consideration [6] and will be briefly introduced in the outlook 4.4.

3 HOMOGENEOUSLY MAGNETIZED NANOPARTICLES

In many applications of high technological relevance, particular in the fields of MEMS- and NEMS-devices, structures of high aspect ratio with one or several dimensions of the system on the nanoscale can be found.

Figure 4: Two-dimensional solution of an array of thin magnetic layers. The colorcode (upper left) indicates the local direction of the magnetization distribution. On small scales, the magnetic distribution follows the shape of the geometry as shown in the inset.

Below a certain size scale, finite size effects occur which allow for the reduction of the three-dimensional system to a lower dimensional approximation.

Magnetic nanoparticles are examples of systems with all dimensions on the nanoscale. In this work, we do not want to study their properties as individual objects but discuss two very relevant applications where they form the basic components within an ensemble of nanoparticles: micron-sized magnetic multi-core beads and self-assembled monolayers.

3.1 Elimination of spatial derivatives

The magnetic exchange coupling does not allow for deviations of the magnetizaton direction on the dimensions of the nanoparticles. Consequently, such particles are homogeneously magnetized. If we further assume a perfectly spherical particle, the resulting external field is given by the dipolar expression [7]

$$\mathbf{H}_{\mathrm{ex}} = \frac{M_{\mathrm{S}} V_{\mathrm{P}}}{4\mu_0} \left(\frac{(\mathbf{r}\cdot\hat{\mathbf{m}})\mathbf{r}}{r^5} - \frac{\hat{\mathbf{m}}}{r^3} \right) \tag{8}$$

while the demagnetization field inside the particle volume is constant and antiparallel to the magnetization of the particle itself, $\mathbf{H}_{\mathrm{d}} = -\frac{1}{3}\mathbf{M}$. Therefore, we have $\mu_0\mathbf{M} \times \mathbf{H}_{\mathrm{d}} = \mathbf{0}$ and demagnetization contributions do not need to be taken into account in this particular case. If we consider a set N such particles, the external magnetic field that the i-th particle feels at its position $\mathbf{r}_i$ is given by the sum of expressions of the form (8)

$$\mathbf{H}_{\mathrm{ex},i} = \sum_{r_{ij}<R} \frac{M_{\mathrm{S},j} V_{\mathrm{P},j}}{4\mu_0} \left(\frac{3(\mathbf{r}_{ij}\cdot\hat{\mathbf{m}}_j)\mathbf{r}_{ij}}{r_{ij}^5} - \frac{\hat{\mathbf{m}}}{r_{ij}^3} \right) \tag{9}$$

with $\mathbf{r}_{ij} = \mathbf{r}_i - \mathbf{r}_j$ and $r_{ij} = |\mathbf{r}_{ij}|$. The cutoff value R is set to $7.5 \times \langle R_{\mathrm{P}} \rangle$, with $\langle R_{\mathrm{P}} \rangle$ the average particle radius of the particle distribution according to [8].

Since the magnetization is constant along each individual magnetic volume, the exchange contribution in

equation (3) is 0 and, therefore, equation (2) no longer contains spatial derivatives. The original set of partial differential equations has been simplified to a set of ordinary ones. If we consider N such particles, the set of equations can be rewritten in matrix form as

$$(\mathsf{Id} - \alpha\mathsf{M})\frac{\partial \mathsf{m}}{\partial t} = \gamma \mathsf{M}\mathsf{H}_{\text{eff}} \tag{10}$$

with Id the identity mapping on $\mathbb{R}^{3N\times 3N}$, M the block diagonal matrix

$$\mathsf{M} = \begin{pmatrix} \mathsf{M}_1 & & 0 \\ & \ddots & \\ 0 & & \mathsf{M}_N \end{pmatrix}$$

with $\mathsf{M}_{n,ij} = \epsilon_{ijk}\hat{m}_{n,k}, n = 1, ..., N$, and

$$\frac{\partial \mathsf{m}}{\partial t} = \frac{\partial}{\partial t}(\hat{m}_{x,1}, \hat{m}_{y,1}, ..., \hat{m}_{x,2}, ...)^T$$
$$\mathsf{H}_{\text{eff}} = (H_{\text{eff},x,1}, H_{\text{eff},y,1}, ..., H_{\text{eff},x,2}, ...)^T.$$

In the subsequent sections, solutions of equation (10) are presented.

3.2 Magnetic multi-core beads

Lab-on-a-chip or μTAS-technologies have evolved to an important branch of MEMS-devices. Biomolecules pass different channel geometries and undergo various chemical procedures on a small microfluidic geometry. In many situations, there is no direct way to monitor or manipulate such molecules. Magnetic beads form an elegant way to label and handle them as they feel a force in an inhomogeneous magnetic field [9] and may also be tracked via their magnetic stray field [10]–[13]. Such beads consist of magnetic nanoparticles embedded in polymer matrix which is usually stabilized by a ligand shell in order to prevent oxidation or other chemical reactions [14], Figure 5(a). Commonly, the nanocomposites are not monodisperse but often follow a log-normal distribution, as was also assumed for the example. We distributed $N = 100$ nanospheres of a mean diameter of 12 nm and a standard deviation $\sigma = 2$ nm along a bead volume with radius $R_S = 50$ nm. The magnetic multi-core bead is assumed to be magnetically saturated at $t = 0$.

Figure 5(c) shows a solution of the magnetic relaxation process. As we can see, for $t \to \infty$, the total magnetic moment goes to 0. These assemblies exhibit a paramagnetic behavior. Even though individual nanoparticles are strongly coupled to each other via their dipolar stray field, the ensemble reaches an equilibrium state of no remanence magnetization. This type of analysis is well suited for the calculation of relaxation dynamics and the prediction of typical demagnetization time constants τ due to dipolar particle coupling [6].

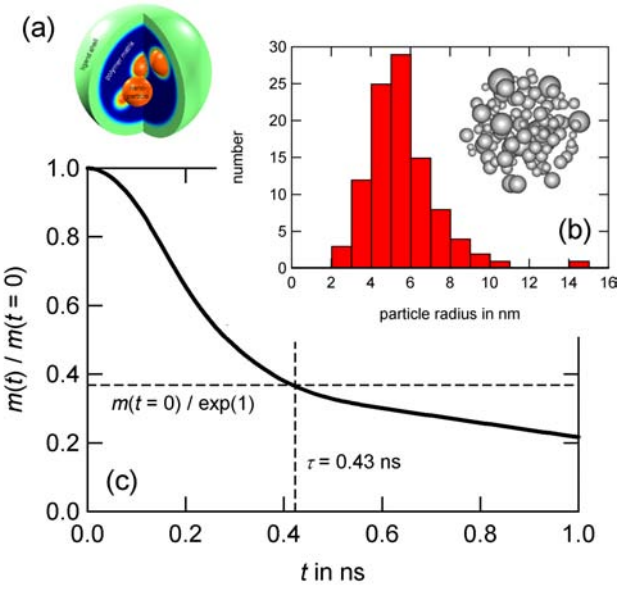

Figure 5: (a) Magnetic bead as an ensemble of magnetic nanoparticles which have a size distribution according to the log-normal function (b). (c) Relaxation of the total magnetic moment m of a magnetic multi-core bead which is brought into saturation at the time $t = 0$.

3.3 Self-assembled monolayers

Three-dimensional arrays of magnetic nanoparticles as discussed in the previous section form an important component in the design of micron-sized superparamagnetic beads. However, a much higher relevance can be found in self-assembled monolayers of magnetic nanocrystalites. Depending on the preparation method, various spatial symmetries can be obtained. An example for particles assembled in a hexagonal structure is shown in Figure 6(a). The absence of exchange coupling results in a very high curvature of the magnetic distribution which minimizes the magnetic field energy of the ensemble.

In contrast to the three-dimensional configurations, these structures have high coercive field which can manipulated by a change of the properties of the nano components themselves. As shown in Figure 6(b), the introduction of a uniaxial anisotropy with a randomly distributed easy axis vector $\hat{\mathbf{k}}$ results in a significant increase of the hysteretic response. Another interesting feature can be found in anisotropic response functions. Figure 6(c) shows the susceptibility calculated from the virgin curves of different assemblies. For more information on these types of devices and their promising fields of applications, see the article *Magnetic Nanoparticles for Novel Granular Spintronic Devices* [15] in these conference proceedings.

Here, we would like to make a short but very helpful sidenote. It is often asked, how to implement a ferromagnetic permeability μ on a continuum by means of an inline function into COMSOL Multiphysics. Well, we

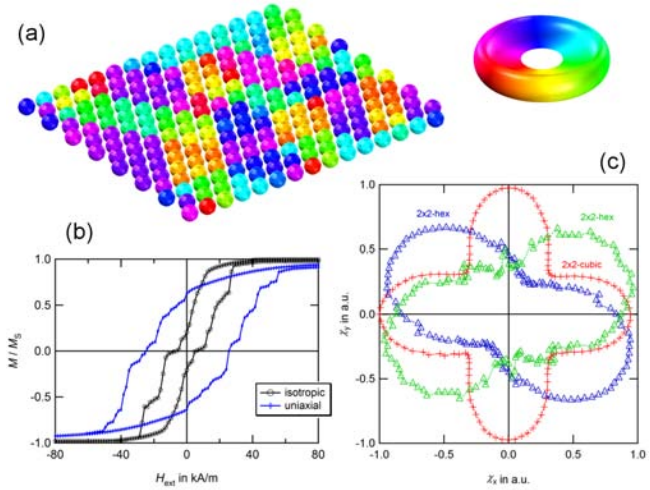

Figure 6: Magnetic properties of a two-dimensional ensemble of hexagonally ordered magnetic nanoparticles. (a) Magnetic equilibrium state, (b) magnetic response functions for isotropic and uniaxial magnetocrystalline anisotropy, (c) susceptibility of virgin curves in dependency of the in-plane magnetic field component.

do not know a good way to use inline functions for this matter, but the implementation of such non-linear hysteretic response works very efficiently by introduction of a set of equations of type (10) for a small number of N. The evaluation takes virtually no calculation time since we only add $2N$ degrees of freedom and the characteristic behavior of the hysteresis loop can easily by modified by changing parameters such as the dipole positions $\mathbf{r}$ or the saturation magnetization M_S.

4 A THIN FILM APPROACH

For the analysis of magnetic nanoparticles, it was possible to employ an analytic solution for the calculation of the magnetic stray field. Now, it would not be exactly correct to say that this is not at all possible for thin magnetic layers as we will explain in section 4.4. However, in order to reach a better understanding of these systems, we will begin our discussion with a more intuitive approach.

4.1 Hybrid 2D-/3D-modeling

Similar as exchange coupling entailed a constant magnetization along the volume of a magnetic nanoparticle, a film thickness of only a few nanometers allows for the approximation of the magnetization by a two-dimensional distribution $\mathbf{M}(\mathbf{r}) = \mathbf{M}(x, y)$. Unfortunately, such a reduction of the system dimensionality is *only* possible for the magnetic configuration but not for the magnetic stray field. The reason for this can be easily understood: if we recast the entire system into a two-dimensional

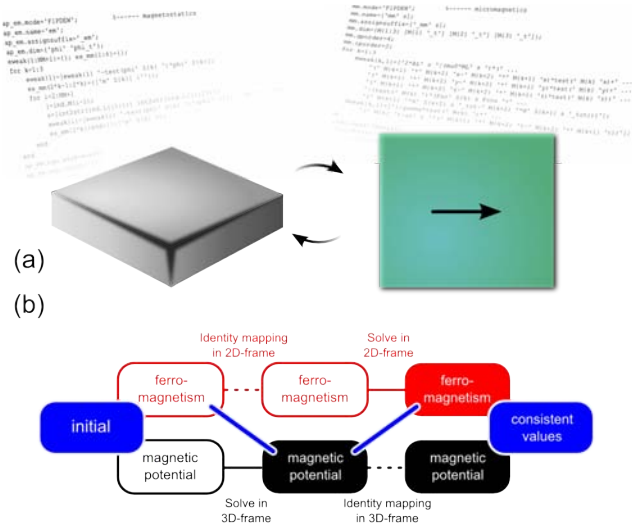

Figure 7: Details on the solution process. (a) Due to its nature, the magnetic stray field is calcualted in a three-dimensional frame and mapped into the two-dimensional layer frame via the projection mapping Φ. (b) Consistent initial values are obtained by starting from a linearly coupled model.

framework, the setup would be symmetric along the z-axis. By this simplification, instead of a thin film, we would analyse the behavior of an infinitely long cuboid under the assumption of a magnetic distribution which does not change in the direction of the symmetry axis. This is exactly the opposite of what we originally intended to analyse. Such a simplification usually results in a higher number of magnetic domains because the demagnetization field is overestimated in comparison to the exchange contribution.

Therefore, we need to work in two different geometry frames: a three-dimensional frame Γ_3 for the calculation of the magnetic potential and a two-dimensional one Γ_2 where we solve for the magnetic degrees of freedom. The frames are connected by a set of extrusion mappings $\Phi_i : \Gamma_3 \to \Gamma_2$, $(x, y, z) \mapsto (x, y)$ with inverse mappings $\Phi_i^{-1} : \Gamma_2 \to \Gamma_3$, $(x, y) \mapsto (x, y, z)$, for every z such that (x, y, z) can be found in the i-th layer. Thus, the magnetization $\hat{\mathbf{m}}$ in the two-dimensional frame is projected onto the three-dimensional layers via $\hat{\mathbf{m}} \circ \Phi_i$, whereas the potential in the two-dimensional coordinate system is given by $\varphi \circ \Phi_i^{-1}$.

A schematic representation of the modeling frame is presented in Figure 7, the mappings Φ and Φ_i^{-1} are implemented via `Extrusion coupling variables`. It should be pointed out that this general formulation of the mapping Φ is compatible with ALE-formalisms and, therefore, it may be easily extended to thin films under stress if additional magnetostrictive contributions need to be taken into account.

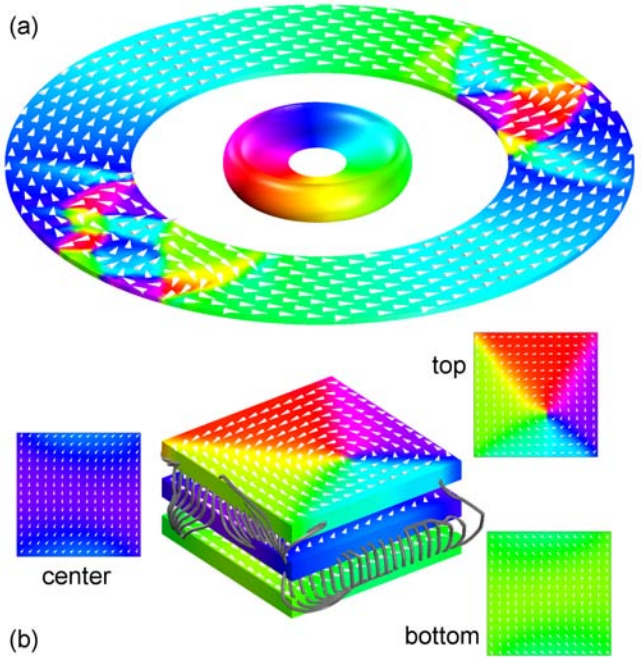

Figure 8: Magnetic multi layer system and resulting magnetic equilibrium states. (a) Magnetic ring, the initial configuration parallel to the x-axis (turquoise) results in a complex magnetic microstructure in minimum and maximum x-regions. (b) Magnetic trilayer, the magnetic equilibrium state minimizes the stray field energy.

4.2 Solver settings

The straight forward implemention of equations (2) to (7) will usually result in the solver error: `Failed to find consistent initial values`, and the solver will be aborted directly at `t=0`. Therefore, in a first step, we need to generate a valid initial configuration. A very good strategy is a sequential presolver step as shown in Figure 7 which assumes only a linear instead of a nonlinear coupling between the two frames for very small time steps: for an arbitrary magnetization distribution, we calculate the magnetic field in the three-dimensional frame. Afterwards, we let the magnetic configuration relax for a small time span in this fixed field configuration. Typically, 1 to 10 ps is a good guess but may depend on the choices of different material parameters. The static field solution together with the end state of the magnetic distribution commonly results in consistent initial values.

4.3 Ferromagnetic thin film arrays

Typical solutions for ferromagnetic thin film systems are shown in Figure 8. Subplot (a) shows the equilibrium state of a magnetic ring. Inner and outer radius are chosen 300 and 500 nm respectively, magnetic parameters are set to $M_S = 1000\,\mathrm{kA/m}$ and $A = 10^{-12}\,\mathrm{J/m}$.

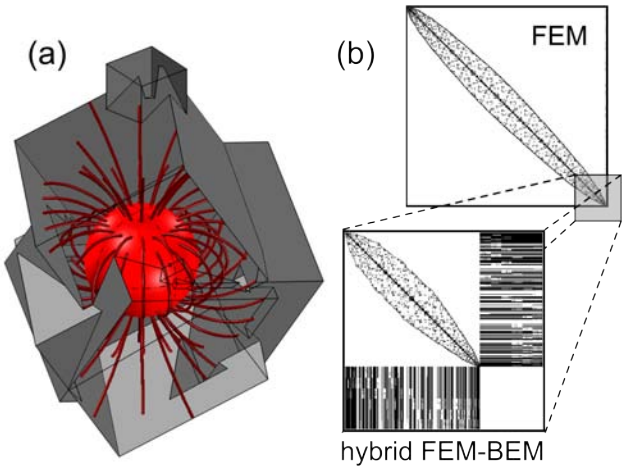

Figure 9: (a) Calculated magnetic field of a homogeneous magnetic sphere by the FEM-BEM approach. (b) Sparsity plots of the resulting system matrices for FEM- and hybrid approach.

The initial state was chosen as $\hat{\mathbf{m}} = \hat{\mathbf{x}}$ which results in magnetic domain structures in maximum and minimum x-regions.

The second example shows a magnetic trilayer with square-shaped layers. The side length is set to 100 nm, magnetization is chosen as $M_S = 1000\,\mathrm{kA/m}$ and exchange constant from top to bottom as $2 \cdot 10^{-12}$, 10^{-11} and $10^{-11}\,\mathrm{J/m}$, respectively. The soft magnetic mater in the top layer allows for the formation of a full vortex state. Center and bottom are magnetically to stiff and, therefore, reach a state of antiparallel alignment, to minimize the magnetic stray field.

4.4 Outlook: Hybrid FEM-BEM method

The calculation of the magnetic potential in a three-dimensional frame as described above introduces a large amount of degrees of freedom in the surronding space of the magnetic object that we are not really interested in. These degrees of freedom can be eliminated in an FEM-BEM framework (**F**inite and **B**oundary **E**lement **M**ethod) which was originally introduced by Fredkin and Koehler [16]. Figure 9(a) shows a solution of the stray field of a homogeneously magnetized sphere in an arbitrary domain. Even though the domain size does not meet the rule of thumb and shows a lot of features along its boundaries, the solution is not affected.

This accuracy of the solution is bought at a cost. Figure 9 shows a sparsity plot of the system matrix for the pure FEM- and for the hybrid FEM-BEM approach. Even though there are far less degrees of freedom to be solved for, the stiffness matrix is a lot denser. This loss of sparsity increases assembly and solving times as well as memory requirements. Whether this approach may

help to increase the performance of our implementation is still to be analyzed.

A rigid introduction to this method and a discussion about advantages and disadvantages can be found in the article *Hybrid FEM-BEM approach for two- and three-dimensional open boundary magnetostatic problems* [6].

CONCLUSION

We have successfully implemented a micromagnetic application mode for the analysis of arrays of ferromagnetic thin films and nanoparticles into COMSOL Multiphysics. In particular, we developed a mixed 2D/3D-framework for the accurate calculation of systems with a high aspect ratio and were able to simplify the original (partial) Landau-Lifshitz-Gilbert equations to a set of ordinary equations for assemblies of magnetic nanoparticles. Also, advanced modeling techniques such as the FEM-BEM coupling have been tested in COMSOL Multiphysics. However, the introduction of boundary integrals result in an increased density of the stiffness matrix which leads to longer solving times and higher memory requirements. Future tests will need to show whether the highly specialized sparse matrix solvers can be adjusted to this set of equations or the proposed 2D/3D-frame will remain the method of choice.

With magnetic thin flims and nanoparticles forming the most relevant components in novel spintronic devices, we believe we have developed a powerful tool for the guidance of future technological developments and the adjustment of a wide range of nanoscaled systems to specified functional tasks.

Acknowledgements

A. Weddemann gratefully acknowledges the financial support of the Alexander von Humboldt foundation.

REFERENCES

[1] P. Grünberg, R. Schreiber, Y. Pang, M.D. Brodsky, H. Sowers. *Layered Magnetic Structures: Evidence for Antiferromagnetic Coupling of Fe Layers across Cr Interlayers.* Phys. Rev. Lett. *57*, 2442-2445, **1986**.

[2] M.N. Baibich, J.M. Broto, A. Fert, F. Nguyen Van Dau, F. Petroff, P. Etienne, G. Creuzet, A. Friederich, J. Chazelas. *Giant Magnetoresistance of (001)Fe/(001)Cr Magnetic Superlattices.* Phys. Rev. Lett. *61*, 2472-2475, **1988**.

[3] A. Weddemann, C. Albon, A. Auge, F. Wittbracht, P. Hedwig, D. Akemeier, K. Rott, D. Meiner, P. Jutzi, A. Hütten. *How to design magneto-based total analysis systems for biomedical applications.* Biosens. Bioelec. *26*, 1152-1163, **2010**.

[4] L.D. Landau, E. Lifshitz. *On the theory of the dispersion of magnetic permeability in ferromagnetic bodies.* Phys. Z. Sowjetunion *8*, 153-169, **1935**.

[5] P.F. Carcia, A.D. Meinhaldt, A. Suna., E.I. du Pont de Nemours and Company *Perpendicular magnetic anisotropy in Pd/Co thin film layered structures.* Appl. Phys. Lett. *47*, 178-180, **1985**.

[6] A. Weddemann, D. Kappe, A. Hütten. *Hybrid FEM-BEM Approach for Two- and Three-Dimensional Open Boundary Magnetostatic Problems.* Proc. COMSOL Conf., Boston, **2011**.

[7] J.D. Jackson in: *Classical Electrodynamics*, 2nd ed., Wiley, New York, **1975**.

[8] A. Weddemann, A. Auge, D. Kappe, F. Wittbracht, A. Hütten. *Dynamic simulations of the dipolar driven demagnetization process of magnetic multicore nanoparticles.* J. Magn. Magn. Mat. *322*, 643-646, **2010**.

[9] A. Weddemann, F. Wittbracht, A. Auge, A. Hütten. *A hydrodynamic switch: Microfluidic separation system for magnetic beads.* Appl. Phys. Lett. *94*, 173501, **2009**.

[10] C. Albon, A. Weddemann, A. Auge, K. Rott, A. Hütten. *Tunneling magnetoresistance sensors for high resolutive particle detection.* Appl. Phys. Lett. *95*, 023101, **2009**.

[11] C. Albon, A. Weddemann, A. Auge, D. Meiner, K. Rott, P. Jutzi, A. Hütten. *Number sensitive detection and direct imaging of dipolar coupled magnetic nanoparticles by tunnel magnetoresistive sensors.* Appl. Phys. Lett. *95*, 163106, **2009**.

[12] A. Weddemann, A. Auge, C. Albon, F. Wittbracht, A. Hütten. *On the resolution limits of tunnel magnetoresistance sensors for particle detection.* New J. Phys. *11*, 113027, **2009**.

[13] A. Weddemann, I. Ennen, A. Regtmeier, C. Albon, A. Wolff, K. Eckstädt, N. Mill, M. Peter, J. Mattay, C. Plattner, N. Sewald, A. Hütten. *Review and outlook: from single nanoparticles to self-assembled monolayer and granular GMR sensors.* Beilstein J. Nanotech. *1*, 75-93, **2010**.

[14] A. Auge, A. Weddemann, B. Vogel, F. Wittbracht, A. Hütten. *A level set based approach for modeling oxidation processes of ligand stabilized metallic nanoparticles.* Appl. Phys. Lett. *96*, 093111, **2010**.

[15] A. Regtmeier, A. Weddemann, I. Ennen, A. Hütten. *Magnetic Nanoparticles for Novel Granular Spintronic Devices - the gGMR sensor.* Proc. COMSOL Conf., Boston, **2011**.

[16] D.R. Fredkin, T.R. Koehler. *Hybrid method for computing demagnetization field.* IEEE Trans. Magn. *26*, 415-417, **1990**.